ISSN: 2414-1895 DOI: 10.6919/ICJE.202410_10(10).0007

Study on the Characteristics of T-type CLC-S Wireless Power Transfer System Suitable for Underwater Charging Equipment

Yunjian Wang[1,2], Sen Yang[1,2, a], Xing Sun[1], Changjie Zhang[1], Ziang Zhu[1], Yunfei Li[1]

[1] School of Electrical Engineering and Automation, Henan Polytechnic University, Jiaozuo 454000, China

[2] Henan Provincial Key Laboratory of Intelligent Detection and Control of Coal Mine Equipment, Jiaozuo 454000, China

[a]E-mail: 332991655@qq.com

Abstract

The power supply of underwater equipment adopts a wireless power supply system that is easy to convert constant voltage and constant current, which can improve the safety of the system. The T-type CLC-S structure wireless power supply system studied in this paper has the characteristics of constant voltage and constant current output, and it is easy to switch the working mode by adjusting the working frequency, without changing the circuit structure or component parameters. In this paper, the conditions for the T-type CLC-S wireless power transmission system to realize the constant current and constant voltage output mode, the transmission power and transmission efficiency in the constant voltage and constant current mode are deduced, the selection of the working point is analyzed, and the transmission characteristics of the system are verified by simulation and experiments, so that the ZPA operation of the inverter can be realized regardless of constant voltage or constant current.

Keywords

MCR-WPT System; CLC-S; Constant Current/Constant Voltage; Change of Frequence.

1. Introduction

In recent years, magnetic coupling resonant wireless power transfer (MCR-WPT) technology has seen rapid development in underwater robots, underwater power inspection and other underwater vehicles. Most underwater vehicles are powered by batteries [4-5], and a charging mode of constant current followed by constant voltage can be used during charging [6], which can effectively shorten the charging time and protect the battery. Reference [7] proposes a T-Π composite resonant network electromagnetic field coupling wireless power transmission system, which utilizes the system's own characteristics to achieve constant output. Reference [8] adds DC-DC converters to both the primary and secondary sides at the same time to achieve constant voltage output and maximum efficiency tracking. Reference [9] analyzes the constant voltage output conditions and the effects of various parameters on them when the T-type CLC-S compensation network resonates. Reference [10] achieves constant current/constant voltage switching output based on the LCC-S structure by phase shifting control. Reference [11] achieves constant current/constant voltage output based on the LCC-LCC/S structure by switching the secondary side topology. Reference [12] increases the AC switch to change the system structure and working frequency, thereby achieving output switching from constant current to constant voltage mode. Although the above references have achieved constant current/constant voltage output, they require switching of electronic switches, which increases the complexity and cost of the system, as well as the loss of the switch tube, and reduces the system

ISSN: 2414-1895 DOI: 10.6919/ICJE.202410_10(10).0007

reliability. The T-type CLC-S resonant network WPT system studied in this paper can easily achieve constant current/voltage output through frequency regulation, and constant voltage output can be achieved with zero phase angle (Zero Phase Angle, ZPA) operation of the inverter output voltage and current.

2. The T-shaped CLC-S Main Circuit of the transmission System

The MC-WPT system for T-shaped CLC-S network is shown in Figure 1, where L_{P1} is the compensation inductor at the transmitter side, L_P and L_S are the inductances of the transmitter coil and the receiver coil, respectively. M is the mutual inductance value, C_{T1} and C_{T2} are the compensation capacitors at the transmitter side, while C_{T3} is the compensation capacitor at the receiver side. R_L is the load resistance, U_{S1} is the DC input voltage, I_{in} is the output current of the inverter, I_P and I_S are the currents of the transmitter and receiver coils, respectively.

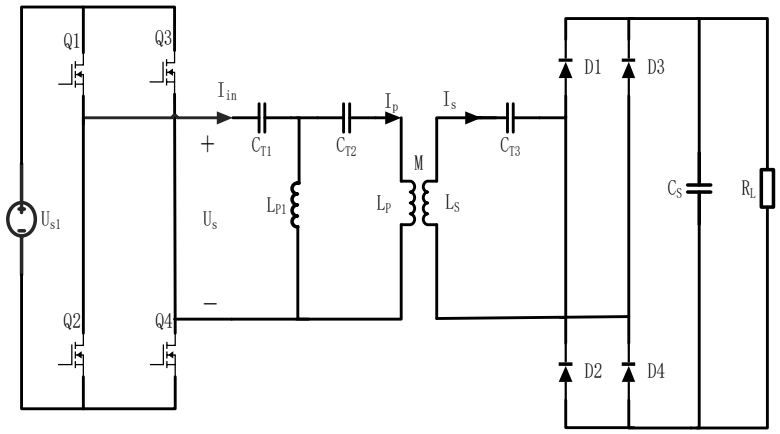

Figure 1. System Main Circuit

The T-type CLC filter is composed of L_{P1}, C_{T1}, and C_{T2}. The system operates as follows:: the full-bridge inverter converts DC voltage into square wave voltage, which undergoes filtration by the T-type filter before being directed to coil L_P to generate sinusoidal current I_P.Subsequently passing through mutual inductor M, the current is received by receiving inductor L_S and supplied to the load via the bridge rectifier circuit. On the receiving side, L_S and C_{T3} operate in resonance with their AC equivalent load denoted as R_{eq}. Treating capacitor C_{T2} as a series connection of $C_{T2a} = C_{T1}$ and C_{T2b} yields the fundamental equivalent circuit shown in Figure 2 from Figure 1; subsequently obtaining the loop current equation based on circuit theory.

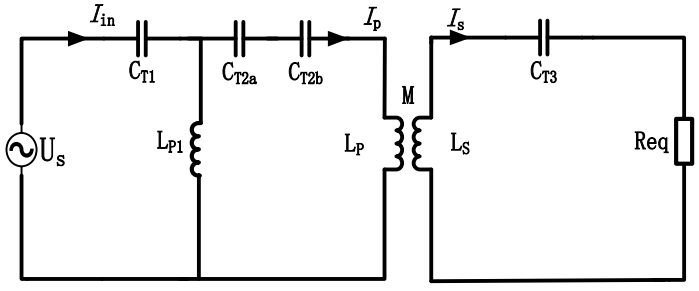

Figure 2. System Equivalent Circuit

ISSN: 2414-1895 DOI: 10.6919/ICJE.202410_10(10).0007

$$\begin{cases} \left(\dfrac{1}{j\omega C_{T1}}+j\omega L_{P1}\right)\times \dot{I}_{in}-j\omega L_{P1}\times \dot{I}_{P}=\dot{U}_{S} \\ \left(-j\omega L_{P1}\right)\times \dot{I}_{in}+\left(\dfrac{1}{j\omega C_{T2}}+j\omega L_{P1}+j\omega L_{P}\right)\times \dot{I}_{P} \\ -j\omega M\times \dot{I}_{S}=0 \\ \left(-j\omega M\right)\times \dot{I}_{P}+\left(\dfrac{1}{j\omega C_{T3}}+j\omega L_{S}+R_{eq}\right)\times \dot{I}_{S}=0 \end{cases} \tag{1}$$

3. Analysis of Transmission Characteristics

Let $\omega_0=1/\sqrt{C_{T2}(L_P+L_{P1})}=1/\sqrt{L_{P1}C_{T1}}=1/\sqrt{L_SC_{T3}}$ represent the resonant frequency of the system, and define normalized frequencies as $\omega_N=\omega/\omega_0$, characteristic impedances as $Z_{T1}=\sqrt{L_{P1}/C_{T1}}$ and $Z_{T3}=\sqrt{L_s/C_{T3}}$,and coefficient as $b=1-C_{T2}/C_{T1}$. Subsequently, equation (1) can be reformulated into:

$$\begin{cases} (1-\omega_N^2)\dot{I}_{in}+\omega_N^2\dot{I}_p=\dfrac{j\omega_N\dot{U}_s}{Z_{T1}} \\ \omega_N^2\dfrac{C_{T2}}{C_{T1}}\dot{I}_{in}+(1-\omega_N^2)\dot{I}_p+\omega_N^2\dfrac{MC_{T2}}{L_{P1}C_{T1}}\dot{I}_s=0 \\ \omega_N^2\dfrac{M}{L_s}\dot{I}_p+(1-\omega_N^2+j\omega_N\dfrac{R_{eq}}{Z_{T3}})\dot{I}_s=0 \end{cases} \tag{2}$$

The currents in each branch can be determined from equation (2) as follows:

$$\dot{I}_{in}=\frac{\dot{U}_S\left(L_{P1}L_sZ_{T3}\left(\frac{1}{\omega_N^4}-\frac{2}{\omega_N^2}+1\right)+M^2Z_{T3}(b-1)+jL_{P1}L_sR_{eq}\left(\frac{1}{\omega_N^3}-\frac{1}{\omega_N}\right)\right)}{A_s} \tag{3}$$

$$\dot{I}_P=\frac{\dot{U}_SL_{P1}L_S(b-1)\left(\dfrac{Z_{T3}}{\omega_N^2}+j\dfrac{R_{eq}}{\omega_N}-Z_{T3}\right)}{A_s} \tag{4}$$

$$\dot{I}_S=\frac{\dot{U}_SL_{P1}MZ_{T3}(1-b)}{A_s} \tag{5}$$

Among these: $A_s=jZ_{T1}Z_{T3}L_PL_sD_2+Z_{T1}L_{P1}L_sR_{eq}D_1$ (6)

$$D_1=b-\frac{2}{\omega_N^2}+\frac{1}{\omega_N^4} \tag{7}$$

$$D_2=k^2(b-1)\left(\frac{\omega_N^2-1}{\omega_N}\right)+\left(\frac{1-b}{b}\right)\left(\frac{3}{\omega_N^3}-\frac{1}{\omega_N^5}-\frac{(2+b)}{\omega_N}+b\omega_N\right) \tag{8}$$

$$k=\frac{M}{\sqrt{L_PL_S}} \tag{9}$$

(1)When $\omega_N=1$ $D_1=b-1$, $D_2=0$,then

ISSN: 2414-1895 DOI: 10.6919/ICJE.202410_10(10).0007

$$\dot{I}_{\mathrm{p}} = j\dot{U}_{\mathrm{s}} / Z_{\mathrm{T1}} \tag{10}$$

$$\dot{I}_{\mathrm{s}} = -\frac{MZ_{\mathrm{T3}}}{L_{\mathrm{s}}R_{\mathrm{eq}}Z_{\mathrm{T1}}}\dot{U}_{\mathrm{s}} \tag{11}$$

$$\dot{I}_{\mathrm{in}} = \frac{M^2 Z_{\mathrm{T3}}}{L_{\mathrm{p1}}L_{\mathrm{s}}Z_{\mathrm{T1}}R_{\mathrm{eq}}}\dot{U}_{\mathrm{s}} \tag{12}$$

At this juncture, the output voltage is $\dot{U}_{R_{\mathrm{eq}}} = \dot{I}_{\mathrm{s}}R_{\mathrm{eq}} = -\frac{MZ_{\mathrm{T3}}}{L_{\mathrm{s}}Z_{\mathrm{T1}}}\dot{U}_{\mathrm{s}}$, independent of the load and operating in a constant voltage output mode. Additionally, $\dot{U}_{\mathrm{s}} / \dot{I}_{\mathrm{in}}$ is a purely real number that enables ZAP operation.

The expression for the output power is as follows:

$$P_{\mathrm{o}} = I_{\mathrm{s}}^2 R_{\mathrm{eq}} = (MZ_{\mathrm{T3}}U_{\mathrm{s}})^2 / (L_{\mathrm{s}}Z_{\mathrm{T1}})^2 R_{\mathrm{eq}} \tag{13}$$

The formula for the transmission efficiency is as follows:

$$\eta = \frac{I_{\mathrm{s}}^2 R_{\mathrm{eq}}}{U_{\mathrm{s}}I_{\mathrm{in}}} = \frac{(\frac{MZ_{\mathrm{T3}}U_{\mathrm{s}}}{L_{\mathrm{s}}Z_{\mathrm{T1}}R_{\mathrm{eq}}})^2 R_{\mathrm{eq}}}{\frac{M}{L_{\mathrm{p1}}}\frac{MZ_{\mathrm{T3}}}{L_{\mathrm{s}}R_{\mathrm{eq}}}\frac{\dot{U}_{\mathrm{s}}}{Z_{\mathrm{T1}}}} = 1 \tag{14}$$

At $D_2 = 0$, with the sole exception of $\omega_{\mathrm{N}} = 1$. There are also two frequency points, as shown in Equation (15). Furthermore, it is capable of maintaining a constant pressure output; however, due to space constraints, further analysis will not be provided.

$$\begin{cases} \omega_{\mathrm{N1}} = \sqrt{\dfrac{\sqrt{bk^2 + (1-b)} + 1}{b(1-k^2)}} \\ \omega_{\mathrm{N2}} = \sqrt{\dfrac{\sqrt{bk^2 + (1-b)} - 1}{b(k^2 - 1)}} \end{cases} \tag{15}$$

(2) When $D_1 = 0$ and $D_2 \neq 0$ are both present, the following can be derived:

$$\begin{cases} \omega_{\mathrm{N4}} = \sqrt{\dfrac{1 + \sqrt{1-b}}{b}} \\ \omega_{\mathrm{N5}} = \sqrt{\dfrac{1 - \sqrt{1-b}}{b}} \end{cases} \tag{16}$$

At this point,

ISSN: 2414-1895 DOI: 10.6919/ICJE.202410_10(10).0007

$$\dot{I}_s = \frac{L_{p1} M (1-b) \dot{U}_s}{j Z_{T1} L_p L_s D_2} \tag{17}$$

$$P_o = \frac{U_s^2 M^2 b^2 L_{p1}^2 R_{eq}}{Z_{T1}^2 L_S^2 L_P^2 \left(\frac{1}{\omega_N^5} - \frac{3}{\omega_N^3} + \frac{2+b-bk^2}{\omega_N} + \left(bk^2 - b\right)\omega_N \right)^2} \tag{18}$$

$$\eta = \frac{k^2 b^2 (1-b)}{\left(\frac{3}{\omega_N^3} - \frac{1}{\omega_N^5} - \frac{2+b-bk^2}{\omega_N} + b\left(1-k^2\right)\omega_N \right) \cdot \left(\frac{1}{\omega_N^3} - \frac{1}{\omega_N} \right)} \tag{19}$$

The input impedance at this constant current frequency is as follows:

$$Z_{in} = \frac{j Z_{T1} Z_{T3} L_P L_S D_2}{L_{P1} L_S Z_{T3} \left(\frac{1}{\omega_N^4} - \frac{2}{\omega_N^2} + 1 \right) + M^2 Z_{T3} (b-1) + j R_{eq} \left(\frac{1}{\omega_N^3} - \frac{1}{\omega_N} \right)} \tag{20}$$

In accordance with Equation (17), the output current is load-independent and operates in a constant current output mode.

4. Establish the Operating Point.

Upon examining Equations (15) and (16), it is evident that the frequency point for achieving constant current and constant voltage output in the system is associated with parameter b. Therefore, when selecting the frequency point, consideration should be given to the value of b in determining the operating frequency. Figures 3 and 4 depict the output current and transmission efficiency of the system under various b values and frequencies in constant current output mode. It can be observed from these figures that while the output current of ω_{N4} is lower than that of ω_{N5} under identical loads, the transmission efficiency of ω_{N4} significantly surpasses that of ω_{N5}. Consequently, based on high efficiency, a working point frequency of ω_{N4} is determined.

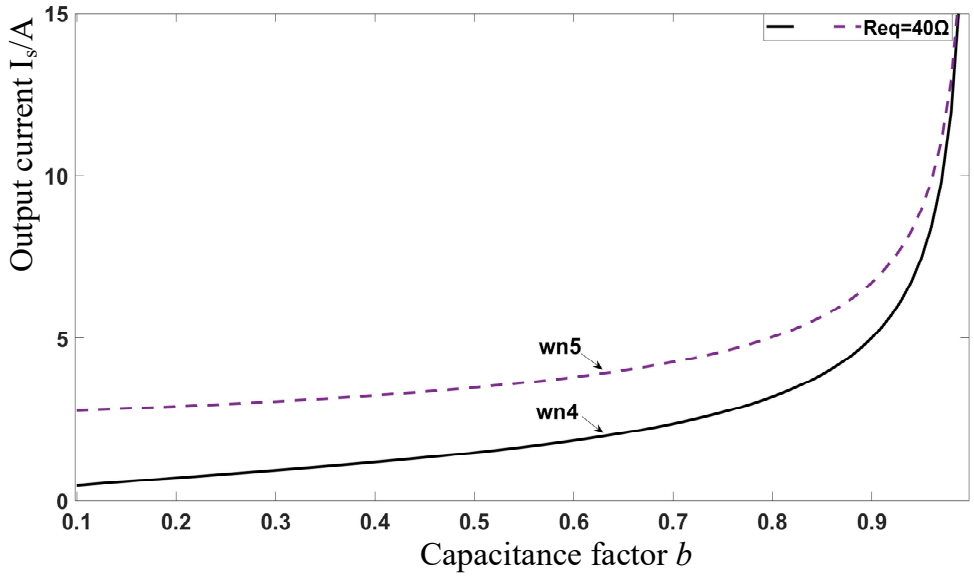

Figure 3. illustrates the impact of the parameter b on the output current.

ISSN: 2414-1895 DOI: 10.6919/ICJE.202410_10(10).0007

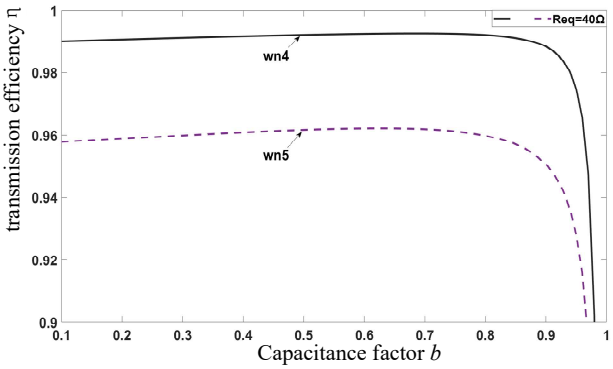

Figure 4. illustrates the impact of the parameter b on transmission efficiency.

At a frequency of ω_{N4}, as b increases from 0.1 to nearly 1, the output current also increases; however, the transmission efficiency is higher at b < 0.92. When b > 0.92, the transmission efficiency decreases rapidly as b increases. In the constant-voltage output mode of $\omega_N = 1$, the transmission efficiency is independent of the output power. Considering all these factors to ensure high-efficiency transmission and large current output, the value of b is taken as 0.9.

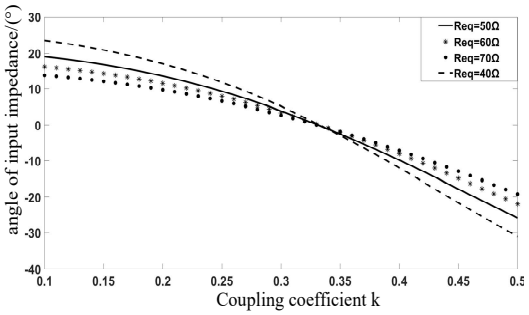

Figure 5. the impact of coupling coefficient on the input impedance angle.

Table 1. Simulation parameters

Parameters	Value	Parameters	Value
U_S/V	48	L_P/μH	145.59
C_{T1}/nF	156.5	L_S/μH	80
C_{T2}/nF	15.65	C_{T3}/nF	31.662
L_{P1}/μH	16.176	R_L/Ω	30-15

Based on the aforementioned analysis, a set of system parameters is designed as detailed in Table 1, with the resonant frequency at $\omega_N = 1$ being 100 kHz.

Based on the parameters in Table 1, Figure 6 illustrates the amplitude-frequency characteristics of the voltage gain in constant-voltage output mode. It can be observed from the figure that there are three frequency points where the voltage gain remains consistent to ensure constant-voltage output, with a transmission efficiency of 1 at these points. The frequency range for constant-voltage output

ISSN: 2414-1895 DOI: 10.6919/ICJE.202410_10(10).0007

is relatively wide and independent of parameter b. Therefore, b is chosen as the system's operating frequency for constant-voltage operation.

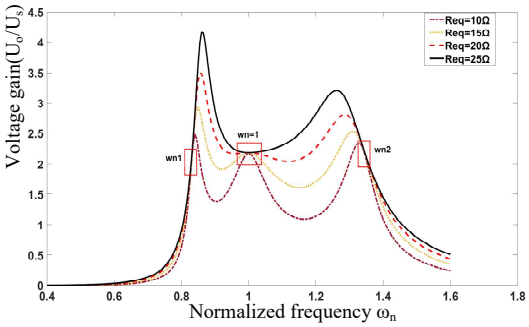

Figure 6. the frequency response of voltage gain (Uo/Us) under various load conditions.

Figure 7 illustrates the amplitude-frequency characteristics of current gain in constant current output mode. It is evident from the graph that there are two frequencies, namely ω_{N4} and ω_{N5}, which satisfy the requirement for constant current output. However, due to higher efficiency, the frequency range for maintaining a constant current output at point ω_{N4} is wider than that at point ω_{N5}. Therefore, selecting point ω_{N4} as the system's operating point is more suitable for the constant current output mode.

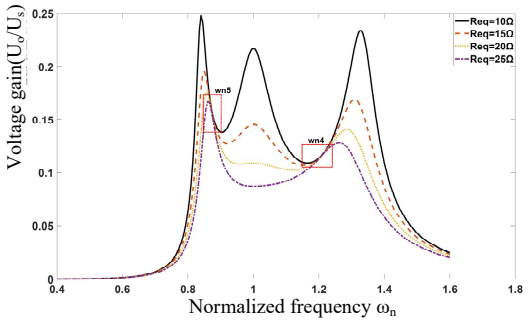

Figure 7. Frequency response of current gain (Is/Us) under varying load conditions.

Underwater wireless power transmission systems commonly employ a V-type coupling mechanism [13], with the mutual inductance coefficient typically being less than 0.5. Consequently, the impact of the coupling coefficient on system performance when it is below 0.5 is depicted in Fig. 8 and Fig. 9. In constant voltage mode, the transmitted power increases as the coupling coefficient rises, and efficiency stabilizes once the coupling coefficient exceeds 0.08, maintaining high levels of transmission efficiency.

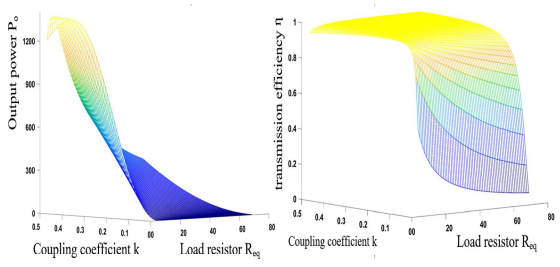

Figure 8. the impact of coupling coefficient on the constant-pressure transmission characteristics.

ISSN: 2414-1895 DOI: 10.6919/ICJE.202410_10(10).0007

Based on Figure 9, it is evident that when 0.4 > 0.1, the system can ensure a specific output power and high transmission efficiency.

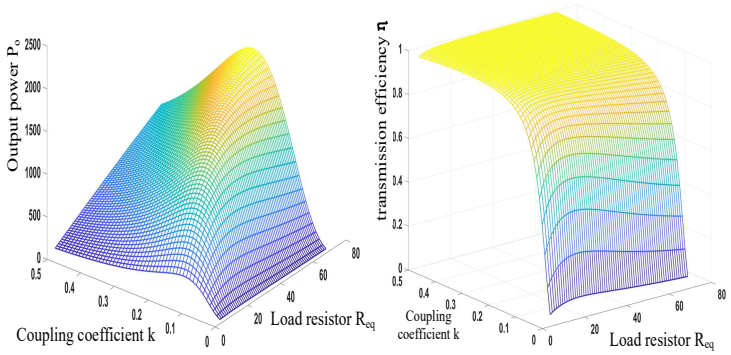

Figure 9. illustrates the impact of the coupling coefficient on the steady-state transmission characteristics.

5. Simulation Analysis

5.1 Constant Current Characteristics Simulation Analysis

In order to verify the constant voltage/current output characteristics of the system and validate the parameter design, a simulation model was developed based on the circuit topology depicted in Figure 1 and utilizing the parameters outlined in Table 1 through MATLAB/Simulink simulation platform as per Equation (1). The subsequent results were obtained from the simulations. The constant current output features of the system were confirmed by load switching. Figures 10 and 11 illustrate simulated voltage and current waveforms of the inverter output under constant current operation with values of R_L =20Ω and R_L =30Ω. It can be observed from these figures that while operating under constant current mode, the system is predominantly within ZPA state; however, there exists a minor phase difference between voltage and current due to slight load variations affecting system resonance marginally, resulting in an overall weakly reactive behavior but having minimal impact on its constant current output characteristics.

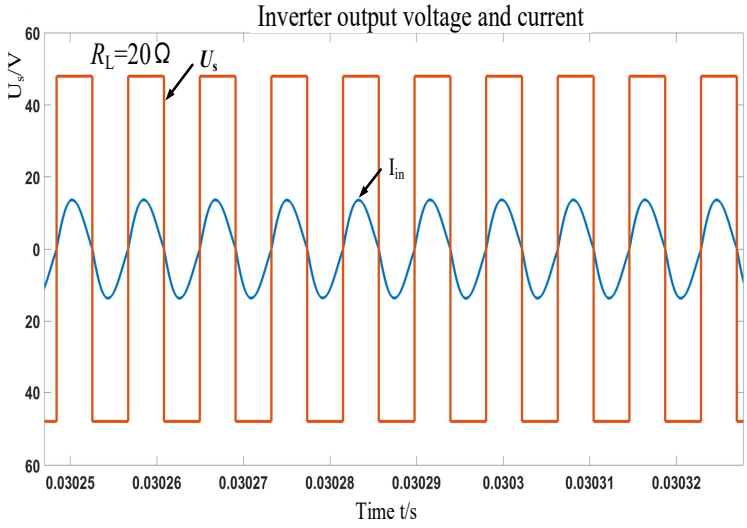

Figure 10. R_L = 20Ω Inverter Output

ISSN: 2414-1895 DOI: 10.6919/ICJE.202410_10(10).0007

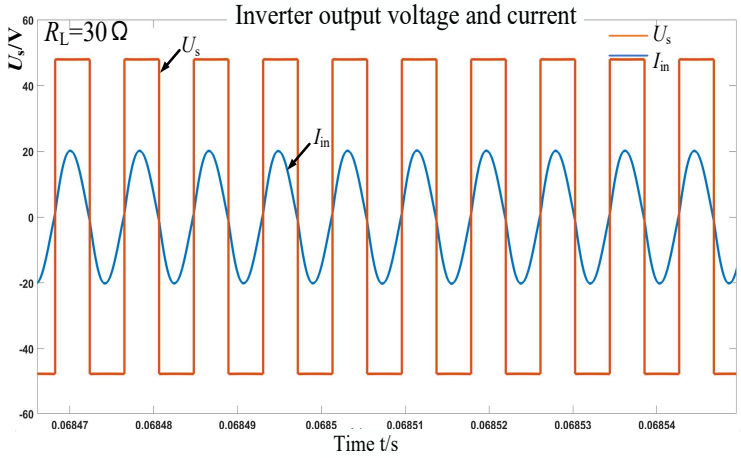

Figure 11. R_L = 30Ω Inverter Output

Figure 12 shows the simulated waveform diagram of the output voltage and output current of the system during operation. The operating frequency is 12.0932 kHZ, and the system operates in constant current mode. At 0.02 seconds, the load R_L switches from 10Ω to 20Ω, and at 0.04 seconds, it switches from 20Ω to 30Ω. From the figure, it can be seen that when the load resistance changes to half of its original value, the output current I_s remains approximately constant in constant current mode, and the output voltage is proportionally reduced, showing good constant current output characteristics.

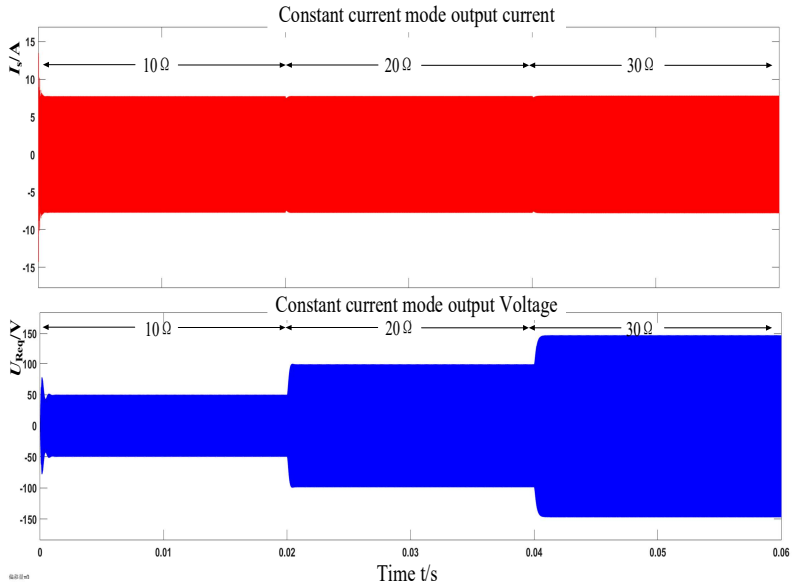

Figure 12. Output Characteristics in Constant Current Mode

5.2 Constant Pressure Characteristics Simulation Analysis

Figures 13 and 14 display the simulation results of the constant voltage mode at a system working frequency of 100kHz. The waveform diagrams for inverter output voltage and current under R_L =20Ω and R_L =30Ω are presented respectively. It is evident from the figures that the phase difference is 0, consistent with the aforementionedformula.

ISSN: 2414-1895 DOI: 10.6919/ICJE.202410_10(10).0007

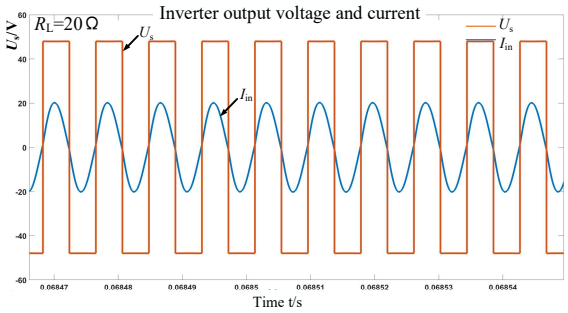

Figure 13. R_L = 30Ω Inverter Output

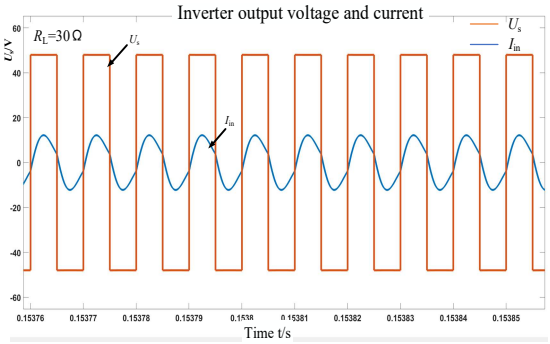

Figure 14. R_L = 30Ω Inverter Output

Figure 15depicts the simulated waveforms of output voltage and current during the power supply process. The system operates in constant voltage mode from 0 to 0.06s; at 0.02s, the load switches from 10Ω to 20Ω, causing a brief fluctuation in voltage before stabilizing; at 0.04s, the load switches from 20Ω to 30Ω, resulting in a minor fluctuation in voltage before remaining unchanged. These results demonstrate that under a varying load of up to 50%, the constant voltage operating mode maintains stable voltage levels, indicating favorable constant voltage output characteristics.

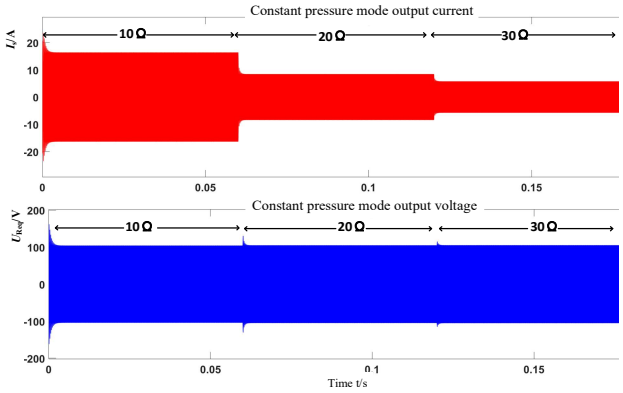

Figure 15. Output Characteristics in Constant Voltage Mode

6. Experimental verification

In order to validate the theoretical analysis presented in this paper, an experimental platform illustrated in Figure 16 was constructed based on the topology depicted in Figure 1, with the STM32F103 utilized as the controller.

ISSN: 2414-1895 DOI: 10.6919/ICJE.202410_10(10).0007

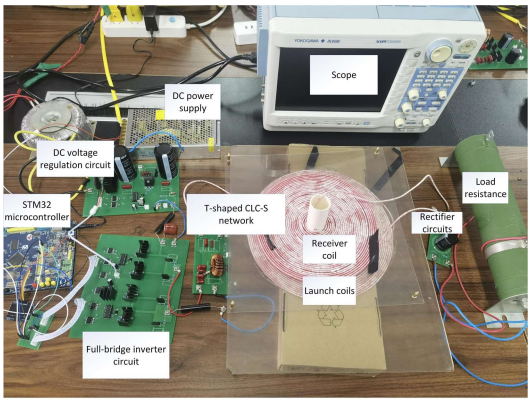

Figure 16. the schematic diagram of the experimental platform.

During simulations, the system characteristics remain consistent with the analysis in the paper when b is set to 0.8 and 0.9, with only minor variations in voltage and current amplitudes. Notably, the current at b=0.9 exceeds that at b=0.8, potentially leading to more significant component heating. Consequently, adjustments are made to the experimental parameters considering safety and component longevity concerns, as detailed in Table 2.

Table 2. Experimental data

Parameters	Value	Parameters	Value
U_S/V	16	L_P/μH	145.59
C_{T1}/nF	69.593	L_S/μH	80
C_{T2}/nF	13.91	C_{T3}/nF	31.662
L_{P1}/μH	36.39	R_L/Ω	30-15

One of the power supplies is regulated to provide a 16V DC voltage, with a filtering capacitor of 470μF. The constant-voltage operating frequency is 100kHz. The constant-current operating frequency can be determined using formula (16) and the aforementioned analysis, resulting in a value of 134.5kHz. The drive waveform for the inverter bridge is generated by the STM32 microcontroller, as depicted in the subsequent figure, where the upper and lower waveforms represent the drive signals for Q1 and Q2, respectively, exhibiting complementary high and low levels.

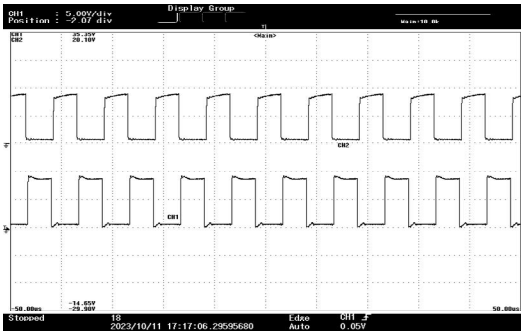

Figure 17. Complementary Waveforms of Inverter

ISSN: 2414-1895 DOI: 10.6919/ICJE.202410_10(10).0007

Figure 18. the relationship between the output voltage and the load in the constant current mode.

Figure 18 illustrates the output voltage of the receiving coil in constant current mode, demonstrating a minimal change of only 0.03A in output current as the load transitions from 20Ω to 15Ω. The measured transmission efficiency is recorded at 90.08%.

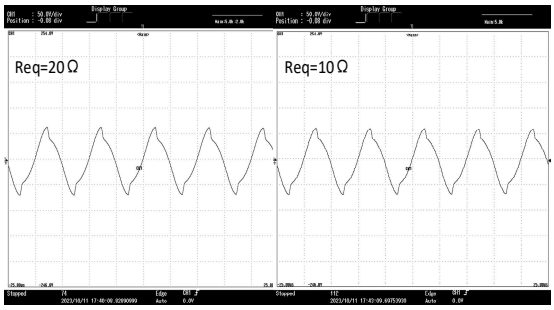

Figure 19. the correlation between output voltage and load in constant voltage mode.

Figure 19 depicts the output voltage of the receiving coil in constant-voltage mode at f=100kHz, where the load is 20Ω and yields an equivalent output voltage to that observed with a 10Ω load. The measured transmission efficiency stands at 91.2%.

7. Conclusion

For underwater robots, sensors, and other specialized underwater equipment, an MCR-WPT system with constant output characteristics (constant current/voltage) is essential. This paper investigates a MCR-WPT system based on a T-type CLC-S resonant network that can easily switch working modes by adjusting the operating frequency. The conditions for achieving constant current and constant voltage outputs are derived and validated through simulation and experimentation. The system under study in this paper offers several advantages: (1) It does not require changes to the topology or complex control circuits; instead, it can switch between working modes by adjusting the operating frequency. (2) Both constant current and constant voltage working modes can operate in ZPA, reducing reactive power loss while enhancing overall system efficiency.

References

[1] LIU Yao, XIAO Jinyu, ZHAO Xiaoling, et al. Review on the development and application of wireless power transmission technology[J].New technology of electrical engineering and electric energy, 2023, 42(02):48-67.

[2] LI Jianpo, LI Shuo, WANG Yijun, et al.A review of magnetic coupling resonant wireless power transfer technology[J]. Electrical Measurement and Instrumentation:1-12.

[3] Huang Renhao, Xie Haonan, Zhang Dongdong, et al. Research on the application of wireless power transmission technology in new power system[J]. Guangxi Electric Power,2022,45(03):1-7+52.

ISSN: 2414-1895 DOI: 10.6919/ICJE.202410_10(10).0007

[4] JHAN Jiayu. Research and design of adaptive underwater wireless energy transfer system[D].University of Electronic Science and Technology of China, 2023.DOI; 10.27005/d.

[5] YAN Zhengchao, HU Qianyu, ZHAO Chenxu, et al.A review of inductive wireless power transfer technology for underwater vehicles[J]. Proceedings of the CSEE:1-16.

[6] Xue Ming, Yang Qingxin, Zhang Pengcheng, et al.Research status and key problems of wireless power transmission technology[J].Transactions of China Electrotechnical Society.

[7] Su Yugang, Xie Shiyun, Tang Chunsen, et al.Constant voltage electric field coupled wireless power transfer system based on T-Π composite resonant network[J].Transactions of China Electrotechnical Society.

[8] Qingbin Chen, Weihao Zhang, Fengchun Ye, et al.A new method for determining the parameters of compensation network with variable constant voltage gain characteristics combined with transformer T network model[J]. Proceedings of the CSEE,2017,3715):4483-4494+4590.

[9] ZHANG Zhen. Design of T-type CLC-S compensation constant voltage inductive coupling energy transfer system[D].Xi'an University of Science and Technology, 2021.DOI:10.27397/d. cnki.gxaku.2020. 000121.

[10] WANG Yunjian, SUN Ping, FAN Xiaoqian, et al. Control of LCC wireless constant current/constant voltage charging system[J]. Manufacturing Automation,2023,45(06):67-70.

[11] Yang Yunhu, Jia Weina, Liang Dazhuang, et al. Transactions of China Electrotechnical Society,2023,38(18):48234837+4852.DOI:10.19595/j.cnki.1000-6753.tces.221236.

[12] LI Qiao. Research on IPT constant current and constant voltage wireless power transmission system based on variable structure and variable frequency [D]. Southwest Jiaotong University, 2021. DOI: 10.27414/d. cnki.gxnju.2020.000922.

[13] Design and implementation of MC-WPT system with wide power range for underwater inspection robot[D].ChongqingUniversity,2022.DOI:10.27670/d.cnki.gcqdu.2022.001095.